# Characterization of Full-Duplex Constant-Envelope Transceiver for Emerging Multifunction Systems

Micael Bernhardt, Jaakko Marin, and Taneli Riihonen

Faculty of Information Technology and Communication Sciences, Tampere University, Finland
e-mail: micael.bernhardt@tuni.fi

***Abstract*—We assess the operation of a special multifunction full-duplex transceiver that uses its frequency-shifting constant-envelope transmitted signal as the downconversion carrier (in contrast to a tone for conventional direct conversion). While self-interference suppression is greatly simplified by using this architecture, the spectra of other downconverted signals turn up sweeping through the frequency domain as the cost of that. Adequate characterization and compensation of these consequences is the key to guarantee the required performance of emerging multifunction systems. We develop solutions to these effects and evaluate the behavior of the transceiver concept by varying transmission- and reception-related parameters.**

***Index Terms*—Jamming, radar, spectrum sensing, full-duplex, frequency-modulated continuous wave (FMCW).**

## I. Introduction

Integrated sensing and communication (ISAC) is a generic concept encompassing spectrum-efficient multifunction systems capable of simultaneously performing communication, sensing, jamming, spectrum monitoring, etc. Prominent beneficiaries of such systems could be, e.g., autonomous vehicles and drone swarms, which need to be able to communicate between the units (viz. data transfer) while simultaneously detecting their relative positions (viz. sensing). [1]–[10]

While there is interest to include ISAC functionality to mobile base stations [11], a cheaper alternative — especially useful in vehicle-to-vehicle situations — is to use a transceiver based on frequency-modulated continuous wave (FMCW) radars. Several studies consider the integration of frequency-shift keying (FSK) modulated data to the FMCW transmit waveform [12]–[14], and it has been shown that this has also the potential to improve radar performance [15]. Combination with other data modulation schemes have been investigated as well [16]. While previous works on ISAC have considered simultaneous data transfer and radar reception in bistatic systems, to the best of our knowledge there is no existing study with a monostatic transceiver, not to mention one based on a correlation receiver.

In this paper, we consider a monostatic radar system that is capable of concurrent radar sensing and wideband signal reception. We analyze and simulate a transceiver (cf. Fig. 1) that uses the transmitted FMCW waveform in the downmixer,

This research work was supported by the Academy of Finland under the grants 315858 "Radio Shield Against Malign Wireless Communication" and 341489/346622 "Multifunctional Radios in Radio-Frequency Systems' Convergence" as well as by the Scientific Advisory Board for Defence.

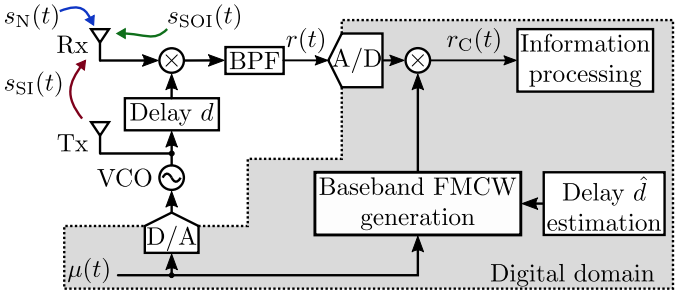


Fig. 1. Block diagram of the proposed multifunction full-duplex transceiver.

which allows for cost-effective radar processing, as well as self-interference (SI) suppression of nearby echoes with a high-pass filter (HPF) — or a band-pass filter (BPF) as in Fig. 1. The signal-of-interest (SOI) in the considered system is a generic orthogonal frequency-division multiplexing (OFDM) signal, which is contained in the received signal alongside the radar echoes. After downmixing with the FMCW signal, the resulting SOI spectrum is non-static and periodically coincides with the filter's stopband. However, with proper system design, the deterioration to the SOI caused by the signal passing through the HPF can be minimized. In our previous publications [17]–[19], we have shown that, by using such a transceiver, we are able to simultaneously support radar sensing and data reception, both conceptually and in practice.

In particular, we examine the tradeoffs of transmit and receive parameters through simulations, which is something where we have only scratched the surface of until now. These parameters include the sweeping frequency of the FMCW waveform and the filter's bandwidth to characterize how they affect the SI suppression and effective signal-to-interference-plus-noise ratio (SINR). We also study effects of time mismatches between the FMCW signals used for downconversion and for compensating the sweeping effect on the received SOI, and neutralization of those effects. With the gained information we are able to define guidelines/limits for the system. We find that it is possible to achieve useful effective SINR levels for the downconverted signals with practical system parameters.

The remainder of the paper is organized as follows. In the following section, we specify our system and signal models in detail. In Section III, we demonstrate the performance of the considered system through simulations. Finally, in Section IV, we present our conclusions.

## II. Multifunction Transceiver

Our proposed system operates according to the block diagram shown in Fig. 1. The monostatic setup can be implemented also with a single shared antenna and a circulator instead of the two closely placed antennas shown in the figure.

### A. Constant-Envelope Waveform

The signal used in the considered system for transmission and downconversion is

$$s_{\mathrm{Tx}}(t) = \mathrm{Re}\left\{s_{\mathrm{J}}(t)\right\}, \tag{1}$$

where $s_{\mathrm{J}}(t) = e^{j2\pi\varphi_{\mathrm{c}}(t)}$ is a constant-envelope FMCW with

$$\varphi_c(t) = f_{\mathrm{c}}t + \varphi(t) = f_{\mathrm{c}}t + \int_0^t \mu(\theta)d\theta. \tag{2}$$

Here $f_{\mathrm{c}}$ is the carrier frequency, and $\varphi(t)$ is a continuous-phase process driven by the generic frequency-modulating waveform

$$\mu(t) = \begin{cases} -\frac{B_{\mathrm{sw}}}{2} + \rho_1\left(t - kT\right), & kT \le t < kT + T_1, \\ \frac{B_{\mathrm{sw}}}{2} - \rho_2\left(t - kT - T_1\right), & kT + T_1 \le t < (k+1)T, \end{cases}$$

for periods $k = 0, 1, 2, \ldots$. Signal $\mu(t)$ has period $T$ divided in the up- and downsweep durations $T_1$ and $T_2$, respectively. These have sweep rates $\rho_1 = {}^{B_{\mathrm{sw}}}/_{T_1}$ and $\rho_2 = {}^{B_{\mathrm{sw}}}/_{T_2}$, with $B_{\mathrm{sw}}$ being the sweeping bandwidth. Without loss of generality, for our subsequent analysis we will consider a symmetric triangular waveform, i.e., $T_1 = T_2 = {}^{T}/_{2}$, which in turn produces $\rho = \rho_1 = \rho_2 = {}^{2B_{\mathrm{sw}}}/_{T}$. Figure 2 depicts the proposed triangular waveform with different delays.

### B. Transceiver Operation

The transmitted signal (1) is captured as self-interference, which is modeled by

$$s_{\mathrm{SI}}(t) = h_{\mathrm{SI}}(t) * s_{\mathrm{Tx}}(t), \tag{3}$$

where $h_{\mathrm{SI}}(t)$ is the SI channel impulse response. This signal is combined over-the-air to the signal-of-interest $s_{\mathrm{SOI}}(t)$ and random noise $s_{\mathrm{N}}(t)$ and downconverted using a delayed version of the multiuse waveform, i.e., $s_{\mathrm{J}}(t-d)$. Delay $d$ is attributable to the non-instantaneous signal propagation within the device. This effect, combined with the fact that multipath reflections of channel $h_{\mathrm{SI}}(t)$ introduce some delay on the transmit signal echoes before arriving at the receive antenna, produces a set of beat frequencies ideally close to direct current (DC) after downconversion. The result of this process is

$$\begin{aligned} r(t) &= \mathcal{F}_{\mathrm{BP}}\left\{e^{-j2\pi\varphi_{\mathrm{c}}(t-d)} \cdot \left(s_{\mathrm{SOI}}(t) + s_{\mathrm{SI}}(t) + s_{\mathrm{N}}(t)\right)\right\} \\ &= s_{\mathrm{I}}(t)\cos\left\{2\pi\left[\varphi_c(t-d) - f_{\mathrm{c}}t\right]\right\} \\ &\quad + s_{\mathrm{Q}}(t)\sin\left\{2\pi\left[\varphi_c(t-d) - f_{\mathrm{c}}t\right]\right\} \\ &\quad - j s_{\mathrm{I}}(t)\sin\left\{2\pi\left[\varphi(t-d) - f_{\mathrm{c}}d\right]\right\} \\ &\quad + j s_{\mathrm{Q}}(t)\cos\left\{2\pi\left[\varphi(t-d) - f_{\mathrm{c}}d\right]\right\} \\ &\quad + \tilde{s}_{\mathrm{SI}}(t) + \tilde{s}_{\mathrm{N}}(t), \end{aligned} \tag{4}$$

where the band-pass filter $\mathcal{F}_{\mathrm{BP}}\{\cdot\}$ is a combination of a low-pass filter designed for suppressing high-frequency components, and a DC block (i.e., a high-pass filter) that eliminates

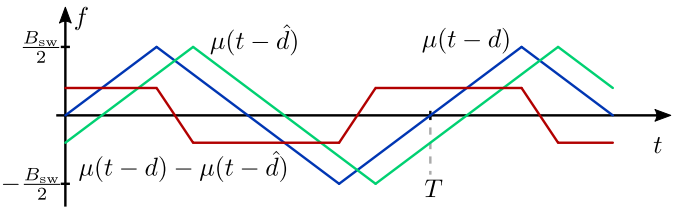


Fig. 2. Triangular waveform $\mu(t)$ used to modulate the frequency of the multifunction signal. Waveforms are shown here with delays $d$ and $\hat{d}$, corresponding to signals used in downconversion and compensation steps, respectively. Their difference, visible as a trapezoidal waveform, causes frequency deviations in the receiver.

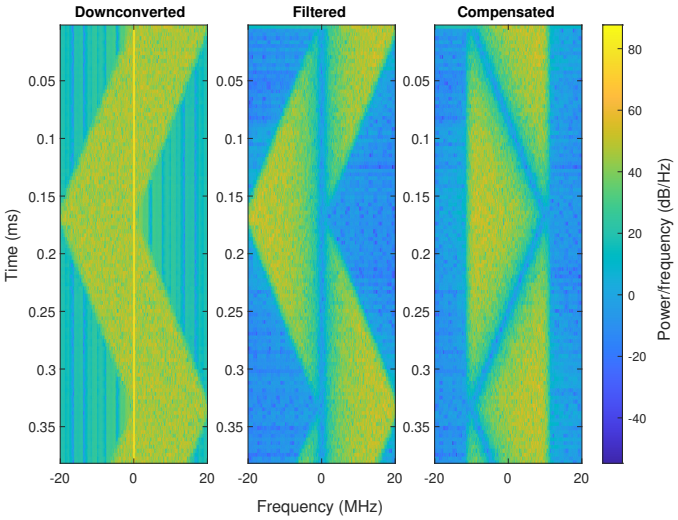


Fig. 3. Spectrograms illustrating different stages of the reception process. From left to right it is shown a SI tone and SOI sweeping in spectrum after downconversion, the result $r(t)$ after filtering, and the signal $r_{\mathrm{C}}(t)$ after sweep compensation.

self-interference beat frequencies, although some of the latter with the highest frequencies might persist and are contained in term $\tilde{s}_{\mathrm{SI}}(t)$. Meanwhile, $\tilde{s}_{\mathrm{N}}(t)$ is the filtered noise, and $s_{\mathrm{I}}(t)$ and $s_{\mathrm{Q}}(t)$ are in-phase and quadrature components of the baseband signal-of-interest, i.e., $s_{\mathrm{BB}}(t) = s_{\mathrm{I}}(t) + j s_{\mathrm{Q}}(t)$.

Due to the varying frequency of the signal used for downconversion in (4), the baseband SOI components will appear moving in spectrum. It is imperative to compensate this effect before attempting any further demodulation or information extraction from them. Figure 3 displays spectrograms of different stages of the reception process. The leftmost one corresponds to downconverted signals before the HPF. The SI is visible therein as the powerful DC component, and the SOI is the wideband signal zig-zagging in spectrum. The center spectrogram shows the result of applying filter in (4) with exaggerated stopband for the purpose of illustration. Compensation of the sweeping movement of the SOI as shown in the rightmost spectrogram is explained shortly.

We can see that the SI suppression filter also nulls useful signal components in a fraction of the SOI's spectrum. Consequently, there is a tradeoff between SI suppression and SOI preservation when selecting the cutoff frequency of the

high-pass portion of filter $\mathcal{F}_{\mathrm{BP}}\{\cdot\}$. If the system's goal is to eliminate all SI beat frequencies, the lower cutoff frequency has to be $f_{\mathrm{low}} \geq \rho\,[\tau_{\max} + \delta]$, where $\tau_{\max}$ is the maximum delay among the relevant paths of SI channel in (3), and $\delta$ is the relative delay between the transmitted waveform and its replica used for downconversion. The latter parameter will become relevant next. The existence of $\rho$ in the condition reveals that the tradeoff is also affected by the transmitted FMCW signal's sweep rate.

### C. Sweep Compensation

Compensation of the sweeping effect after downconversion (4) is done by multiplying $r(t)$ by the baseband multifunction signal $e^{j2\pi\varphi(t-\hat{d})}$ delayed by an estimate $\hat{d}$ of actual delay $d$. After this, we obtain

$$
\begin{aligned}
r_{\mathrm{C}}(t) &= e^{j2\pi\varphi(t-\hat{d})} \cdot r(t) && (5)\\
&= s_{\mathrm{I}}(t)\cos\left\{2\pi\left[\Delta\left(t,d,\hat{d}\right) - f_{\mathrm{c}}d\right]\right\} && (6)\\
&\quad + s_{\mathrm{Q}}(t)\sin\left\{2\pi\left[\Delta\left(t,d,\hat{d}\right) - f_{\mathrm{c}}d\right]\right\} && (7)\\
&\quad - j s_{\mathrm{I}}(t)\sin\left\{2\pi\left[\Delta\left(t,d,\hat{d}\right) - f_{\mathrm{c}}d\right]\right\} && (8)\\
&\quad + j s_{\mathrm{Q}}(t)\cos\left\{2\pi\left[\Delta\left(t,d,\hat{d}\right) - f_{\mathrm{c}}d\right]\right\} && (9)\\
&\quad + \tilde{s}_{NSI}(t).
\end{aligned}
$$

Here $\tilde{s}_{NSI}(t)$ represents noise and self-interference, i.e.,

$$\tilde{s}_{NSI}(t) = e^{j2\pi\varphi(t-\hat{d})} \cdot \left(\tilde{s}_{\mathrm{SI}}(t) + \tilde{s}_{\mathrm{N}}(t)\right),$$

and $\Delta(t,d,\hat{d})$ is the difference between two continuous-phase processes with delays $d$ and $\hat{d}$, calculated as

$$
\begin{aligned}
\Delta\left(t,d,\hat{d}\right) &= \varphi(t-d) - \varphi(t-\hat{d}) && (10)\\
&= \begin{cases} \pm\left\{\rho\left(t(\hat{d}-d) + \frac{d^2-\hat{d}^2}{2}\right) + \frac{B_{\mathrm{sw}}}{2}(d-\hat{d})\right\} \\ \pm\left\{\rho t^2 - \left[\rho\left(d+\hat{d}\right) + B_{\mathrm{sw}}\right]t \right. \\ \qquad \left. + \frac{\rho\left(d^2+\hat{d}^2\right)+B_{\mathrm{sw}}\left(d+\hat{d}\right)}{2}\right\}. \end{cases}
\end{aligned}
$$

The four alternatives for (10) are due to the possible combinations of sweep directions of the FMCW waveforms of downconversion and compensation. The difference between instantaneous frequencies of the phase processes in (10) can be observed in Fig. 2.

If the estimated delay $\hat{d}$ is equal to the actual delay $d$, (10) is simplified to the two first possible expressions. Consequently, terms (7) and (8) are equal to zero, and the sum of (6) and (9) would be equal to $s_{\mathrm{BB}}(t)$. Otherwise, the compensated SOI components will evidence a residual variable frequency difference whose maximum magnitude is equal to $\Delta f = \rho|\hat{d} - d|$. This effectively represents a time-varying carrier frequency offset (CFO). The relative delay between sweep waveforms can be estimated using the received SOI as an auxiliary signal, as shown in [19]. In next section, we present the evaluation of the performance of our receiver under this impairment, in addition to the delay estimation for several FMCW waveform and transceiver parameters.

TABLE I
SIGNAL PARAMETERS

| **Self-interference** | **FMCW signal** | | |
|---|---|---|---|
| | ***Symbol*** | ***Values*** | ***Unit*** |
| Sweep frequency | $f_{\mathrm{sw}} = 1/T$ | 5, 10, 25, 50, 100, 250, 500 | kHz |
| Carrier frequency | $f_{\mathrm{c}}$ | 2.4 | GHz |
| Sweep bandwidth | $B_{\mathrm{sw}}$ | 20 | MHz |
| Sweep delay[a] | $d$ | 0 to 10 | ns |
| Received power | $P_{\mathrm{SI}}$ | $-30$ to 0 | dB |
| **Signal-of-interest** | **OFDM waveform** | | |
| | ***Symbol*** | ***Values*** | ***Unit*** |
| Carrier frequency | $f_{\mathrm{c}}$ | 2.4 | GHz |
| FFT size | $N$ | 1024 | |
| Bandwidth | $B$ | 20 | MHz |
| Cyclic prefix | $L_{\mathrm{cp}}$ | 12.8 | µs |
| Modulation order | $M$ | 4 (QPSK) | |
| Received power | $P_{\mathrm{SOI}}$ | $-50$ to 0 | dB |

[a] Applied to the downconversion waveform.

## III. System Evaluation

We tested our transceiver's performance by means of simulations under different SI and SOI signal parameters shown in Table I. We present the effective SINR obtained for the received and shift-compensated signal (5) as a way to provide generic results applicable to diverse implementations. Our results were obtained from averaging 100 realizations of the experiments. The self-interference channel was modeled as Rician fading with factor $K = 3$, and five uniformly spaced path delays equal to $0.1\,\mu$s, $0.25\,\mu$s, $0.4\,\mu$s, $0.55\,\mu$s and $0.7\,\mu$s. This was chosen to induce SI beat frequencies with values which span from $20\,$kHz to $14\,$MHz depending on the FMCW sweep frequencies of Table I. The SI-suppression HPF was modeled as a DC block [20], whose bandwidths were selected between $1\,$kHz and $10\,$MHz to resemble values of commercially available devices. The cutoff frequency for the low-pass filter was set to $3\,$GHz.

Figure 4 (a) shows the SI suppression performance achieved by our system under different sweep frequencies and DC block bandwidths, without delays between downmixing and compensation FMCW waveforms. The response for a conventional receiver, i.e. without any SI suppression, is also shown as reference. The results demonstrate that the different DC blocks suppress a considerable amount of the interference in high SI power regimes. Unsurprisingly, the highest sweep rates demand larger blocking bandwidths to suppress tones with greater beat frequencies and hence show an improvement with respect to a conventional receiver. For weaker SI signals, the system seems to become limited by a factor different than the SI, evidenced by the curves approaching an horizontal asymptotic limit. For lower sweep rates, increasing the blocking bandwidth beyond a value that suppresses the relevant highest-frequency SI tones does not provide any further advantages. This is more evident when SI power is similar or lower than that of the signal-of-interest, where DC blocks with smaller bandwidths provide better performance. This is due to their decreased effect of spectral nulling on the SOI, which becomes the dominant performance limitation in these regimes.

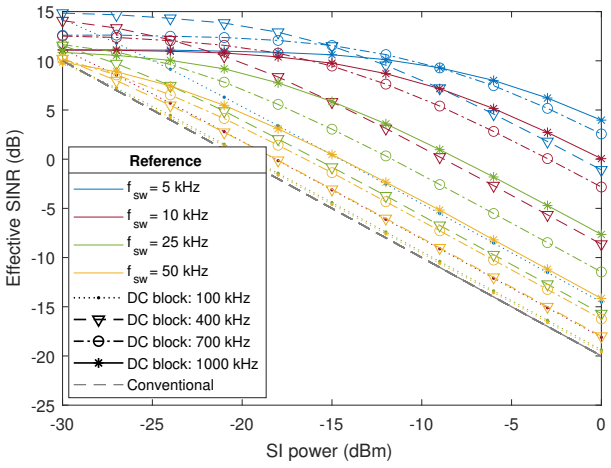


(a)

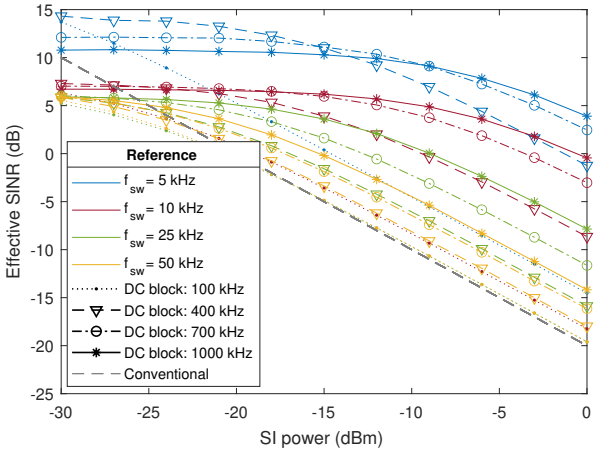


(b)

Fig. 4. Effective SINR vs. self-interference power, for varying FMCW sweep frequency $f_{\mathrm{sw}}$ and DC block bandwidths. SOI power is $-20\,\mathrm{dBm}$, whereas noise power $P_{\mathrm{N}}$ is $-60\,\mathrm{dBm}$. Figure (a) has no delay between downmixing and compensation waveforms, whereas (b) shows results when delay is $6\,\mathrm{ns}$.

Figure 4 (b) depicts the performance when there is a delay of $6\,\mathrm{ns}$ between downconversion and compensation FMCW waveforms. We see that overall performance degrades with respect to previous case by several decibels, especially in the lower SI power regime, except for when $f_{\mathrm{sw}} = 5\,\mathrm{kHz}$. In this case, the sweep delay estimation behaves correctly and achieves compensation of the frequency deviations.

We illustrate the self-interference suppression achieved by the DC blocks in Fig. 5. This plot shows the magnitude response of several filters contrasted with the SI beat frequencies observed for one realization of our channel model when $f_{\mathrm{sw}} = 10\,\mathrm{kHz}$. In this case, it is evident that the narrowest bandwidth would fail to suppress the strongest tone located at $220\,\mathrm{kHz}$ after downconversion. Larger DC block bandwidths guarantee eliminating all SI components, but also a non-negligible portion of the SOI is attenuated, and the effective SINR decreases as shown previously.

Effects of differences in the relative phases of the downmixing and compensation sweep waveforms can be seen in

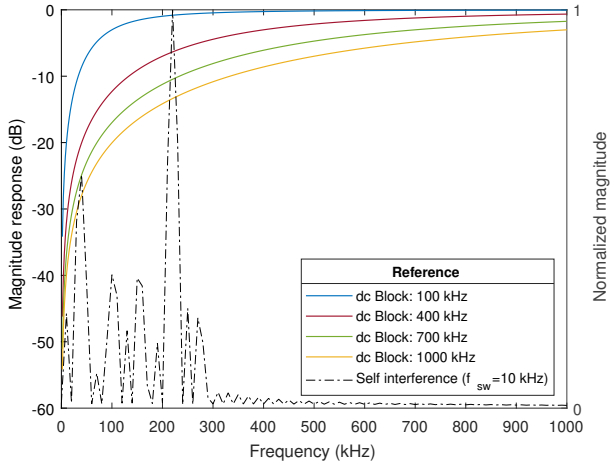


Fig. 5. DC block magnitude responses, and SI beat frequencies obtained after downconversion for a realization of the channel when $f_{\mathrm{sw}} = 10\,\mathrm{kHz}$.

Fig. 6. We observe that larger differences in the relative time positions of those signals induce more degradation in the received signals, even when the delay is a very small fraction of the FMCW signal period. Estimation and correction of this sweep delay greatly improves performance, as shown in Fig. 6 (b) for $f_{\mathrm{sw}} = 5\,\mathrm{kHz}$. As discussed before, a DC block with bandwidth equal to $100\,\mathrm{kHz}$ seems insufficient for eliminating SI in this case. Also, the accuracy of estimate $\hat{d}$ of the delay is not good enough for higher sweep frequencies depicted. This is in line with our results in [19], where we show that high sweep rates might introduce ambiguity in the estimation.

The presence of the DC block does not display effects on the delay estimation performance, even for very low SOI power levels. This is shown in Fig. 7, where we see that for $f_{\mathrm{sw}} = 5\,\mathrm{kHz}$ the residual frequency deviation after estimation and compensation of the delay is less than $1\,\mathrm{kHz}$, and this result does not vary with different DC block bandwidths. The same can be observed for $f_{\mathrm{sw}} = 10\,\mathrm{kHz}$ and $25\,\mathrm{kHz}$, although the higher sweep frequency causes the residual CFO to be larger in these cases. This reinforces the fact that it is recommended to estimate the delay $\hat{d}$ with lower sweep frequencies.

## IV. Conclusion

We investigated the performance tradeoffs obtained for a multiuse full-duplex transceiver inspired by FMCW radar operation. We show through numerical results that this transceiver facilitates self-interference suppression after downconversion, and that it is also possible to simultaneously acquire other signals in spectrum. However, selection of system parameters such as FMCW sweep rate, as well as SI suppression filters, has to be done knowingly since SOI acquisition might be degraded by the self-interference canceler. Specifically, suppression bandwidths should not be much greater than the the product between sweep rate and the largest delay of the relevant SI channel path responses. We also showed that strict synchronization is necessary between downconversion and compensation FMCW waveforms to minimize frequency

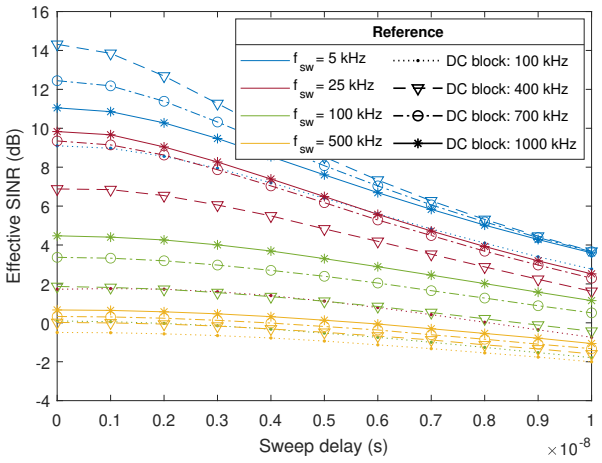


(a)

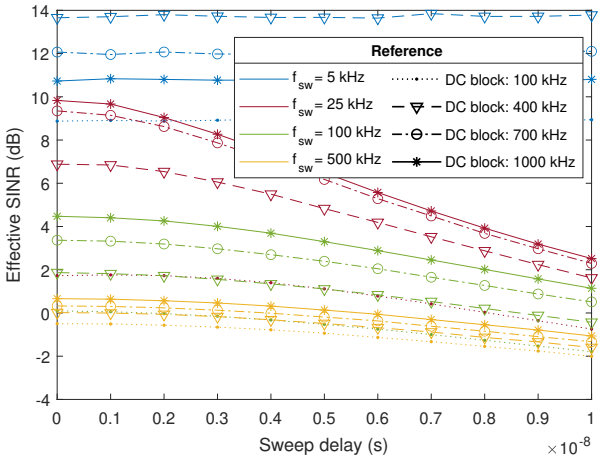


(b)

Fig. 6. Effects of difference in the downconversion and sweep compensation signal delays, for different FMCW sweep frequencies $f_{\mathrm{sw}}$ and DC block bandwidths, and for a system without (a) and with compensation (b). SOI power is $-10\,\mathrm{dBm}$, SI power is $0\,\mathrm{dBm}$ and noise power is $-60\,\mathrm{dBm}$.

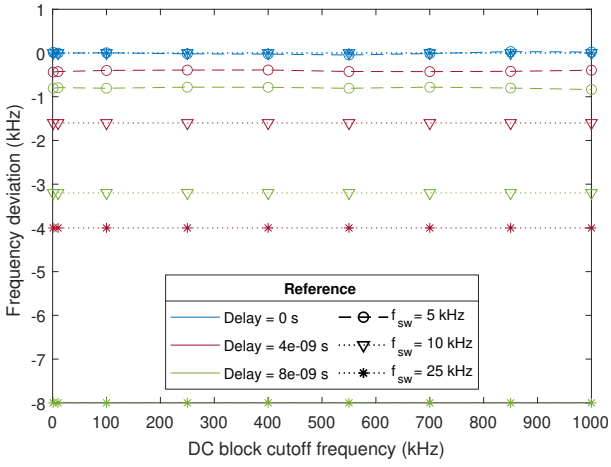


Fig. 7. Residual frequency deviation versus DC block bandwidth, for $f_{\mathrm{sw}} = 5\,\mathrm{kHz}$ and $25\,\mathrm{kHz}$ and three different sweep delays. SOI power is $-40\,\mathrm{dBm}$, SI power is $0\,\mathrm{dBm}$ and noise power is $-60\,\mathrm{dBm}$.

deviations in the downconverted SOI, and that estimation of the delay between those waveforms is not compromised by the transceiver's principle of operation.

## References


[1] N. C. Luong *et al.*, "Radio resource management in joint radar and communication: A comprehensive survey," *IEEE Communications Surveys and Tutorials*, vol. 23, no. 2, pp. 780–814, Apr. 2021.

[2] J. A. Zhang *et al.*, "An overview of signal processing techniques for joint communication and radar sensing," *IEEE Journal on Selected Topics in Signal Processing*, vol. 15, no. 6, pp. 1295–1315, Sep. 2021.

[3] A. Liu *et al.*, "A survey on fundamental limits of integrated sensing and communication," *IEEE Communications Surveys Tutorials*, Feb. 2022.

[4] B. Paul, A. R. Chiriyath, and D. W. Bliss, "Survey of RF communications and sensing convergence research," *IEEE Access*, vol. 5, pp. 252–270, Dec. 2017.

[5] A. Hassanien, M. G. Amin, E. Aboutanios, and B. Himed, "Dual-function radar communication systems: A solution to the spectrum congestion problem," *IEEE Signal Processing Magazine*, vol. 36, no. 5, pp. 115–126, Sep. 2019.

[6] F. Liu *et al.*, "Joint radar and communication design: Applications, state-of-the-art, and the road ahead," *IEEE Transactions on Communications*, vol. 68, no. 6, pp. 3834–3862, Feb. 2020.

[7] F. Liu and C. Masouros, "A tutorial on joint radar and communication transmission for vehicular networks—part II: State of the art and challenges ahead," *IEEE Communications Letters*, vol. 25, no. 2, pp. 327–331, Sep. 2021.

[8] A. Herschfelt, A. R. Chiriyath, S. Srinivas, and D. W. Bliss, "An introduction to spectral convergence: Challenges and paths to solutions," in *Proc. 1st IEEE International Online Symposium on Joint Communications and Sensing*, Feb. 2021.

[9] Z. Feng *et al.*, "Joint radar and communication: A survey," *China Communications*, vol. 17, no. 1, pp. 1–27, Jan. 2020.

[10] L. G. de Oliveira *et al.*, "Joint radar-communication systems: Modulation schemes and system design," *IEEE Transactions on Microwave Theory and Techniques*, vol. 70, no. 3, pp. 1521–1551, Nov. 2021.

[11] C. Baquero Barneto *et al.*, "Full-duplex OFDM radar with LTE and 5G NR waveforms: Challenges, solutions, and measurements," *IEEE Transactions on Microwave Theory and Techniques*, vol. 67, no. 10, pp. 4042–4054, Aug. 2019.

[12] C. Yang, M. Wang, L. Zheng, and C. Tang, "Dual function system with shared spectrum using FMCW," *IEEE Access*, vol. 6, pp. 79 026–79 038, May 2018.

[13] W. Scheiblhofer *et al.*, "In-chirp FSK communication between cooperative 77-GHz radar stations integrating variable power distribution between ranging and communication system," *International Journal of Microwave and Wireless Technologies*, vol. 8, no. 4-5, pp. 825–832, Feb. 2016.

[14] C. H. Wang and O. Altintas, "Demo: A joint radar and communication system based on commercially available FMCW radar," in *Proc. IEEE Vehicular Networking Conference*, Dec. 2018.

[15] M. H. Li, K. Ju Wu, and C. L. Yang, "Multi-target monitoring for distinguishable range improvement using a hybrid FMCW-FSK 24 GHz radar," in *Proc. International Symposium on Antennas and Propagation*, Oct. 2021.

[16] D. Ma *et al.*, "FRaC: FMCW-based joint radar-communications system via index modulation," *IEEE Journal on Selected Topics in Signal Processing*, vol. 15, no. 6, pp. 1348–1364, Oct. 2021.

[17] J. Marin, M. Bernhardt, and T. Riihonen, "Full-duplex multifunction transceiver with joint constant envelope transmission and wideband reception," in *Proc. IEEE International Conference on Acoustics, Speech and Signal Processing*, Jun. 2021.

[18] J. Marin, M. Bernhardt, M. Heino, and T. Riihonen, "Monostatic FMCW radar architecture for multifunction full-duplex radios," in *Proc. Asilomar Conference on Signals, Systems, and Computers*, Nov. 2021.

[19] M. Bernhardt, J. Marin, and T. Riihonen, "Estimation of receiver frequency deviations in multifunction frequency-modulating transceivers," in *Proc. IEEE Vehicular Technology Conference*, Jun. 2022.

[20] K. Tittelbach-Helmrich, "Digital DC blocker filters," *Frequenz*, vol. 75, no. 9-10, pp. 331–339, feb 2021.